MIXED GAS CONCENTRATION INVERSION BASED ON THE ULTRAVIOLET ABSORPTION SPECTRUM BY A HIERARCHICAL CONVOLUTIONAL NEURAL NETWORK**

C. Lu*, Y. Bian, X. Hu, S. Jin, Y. Huang, Y. Cui

Advanced Photonics Center, School of Electronic Science & Engineering at Southeast University, Nanjing, Jiangsu, China; e-mail: changguilu@seu.edu.cn

A hierarchical convolutional neural network (CNN) model for mixed gas concentration inversion is proposed. In our experiment, mixtures of SO_2, NO_2, and NH_3 were analyzed. SO_2 and NO_2 were the detected gases, while NH_3 was the interfering gas. For the simulation samples, the average absolute errors were 0.5 and 0.9 ppm for SO_2 and NO_2, respectively. For the experimental samples, the model performed well when the absorption intensities of components differed by no more than one order of magnitude. Compared with the single-module CNN model without a hierarchical structure, the results demonstrate that the hierarchical structure reduces cross-interference and improves the prediction accuracy to a great extent. We believe that our model will have a promising application in the field of gas detection.

Keywords: *spectral analysis, hierarchical convolutional neural network, gas detection.*

ИНВЕРСИЯ КОНЦЕНТРАЦИИ СМЕШАННОГО ГАЗА НА ОСНОВЕ УЛЬТРАФИОЛЕТОВОГО ПОГЛОЩЕНИЯ С ПОМОЩЬЮ ИЕРАРХИЧЕСКОЙ СВЕРТОЧНОЙ НЕЙРОННОЙ СЕТИ

C. Lu*, Y. Bian, X. Hu, S. Jin, Y. Huang, Y. Cui

УДК 543.42

Центр передовой фотоники, Школа электронных наук и инженерии Юго-Восточного университета, Нанкин, Цзянсу, Китай; e-mail: changguilu@seu.edu.cn

(Поступила 11 октября 2021)

Предложена модель иерархической сверточной нейронной сети (CNN) для инверсии концентрации смешанного газа. Проанализированы смеси SO_2, NO_2 и NH_3, где SO_2 и NO_2 — исследуемые газы, NH_3 — "мешающий" газ. Для образцов моделирования получены средние абсолютные ошибки 0.5 и 0.9 ppm для SO_2 и NO_2. Модель хорошо зарекомендовала себя при различиях интенсивности поглощения компонентов не более чем на порядок. По сравнению с одномодульной моделью результаты CNN без иерархической структуры демонстрируют, что иерархическая структура значительно снижает перекрестные помехи и повышает точность прогнозирования.

Ключевые слова: *спектральный анализ, иерархическая сверточная нейронная сеть, обнаружение газа.*

Introduction. The detection of gas mixtures has a wide range of applications in many areas. For example, noninvasive disease diagnosis can be achieved by analyzing the exhaled breath because more than a hundred diseases are associated with human exhalation. Through real-time evaluation of hazardous gases in mines, the safety of operations could be improved. In addition, environmental protection can be effectively carried out through the monitoring of air pollutants [1]; however, the detection of gas mixtures is disturbed by the cross-interference between different components [2–5]. Strong absorption gas would especially have a serious overlap with a weak one, and this situation needs to be resolved urgently [6, 7].

**Full text is published in JAS V. 89, No. 4 (http://springer.com/journal/10812) and in electronic version of ZhPS V. 89, No. 4 (http://www.elibrary.ru/title_about.asp?id=7318; sales@elibrary.ru).

The most common methods for gas detection include chemical and optical measurements. Chemical measurements have the advantages of a simple principle and a convenient operation [8, 9]. However, these methods are easily affected by the detecting environment and fail to achieve continuous measurement for a long time. Optical measurements predict concentrations by analyzing gas absorption spectra [10, 11]. They have a wider range of applications due to their high accuracy and non-contact capabilities – for example, tunable diode laser absorption spectroscopy (TDLAS) uses a near-infrared tunable laser diode as the light source to analyze the absorption lines at specific wavelengths [12, 13], a method that is accurate and stable, but more expensive. Since most gases have strong absorption peaks in the ultraviolet band, this band is widely used for gas detection [14, 15] for example, differential optical absorption spectroscopy (DOAS) performs analysis by the narrow-band absorption of molecules in the ultraviolet band [16, 17], while the ultraviolet fluorescence method uses ultraviolet light to excite fluorescent substances and then analyzes the generated fluorescence spectrum [18–20]. These two methods a more inexpensive and have higher precision, but the detectable types of gases are limited [21, 22].

Due to the limitations of traditional methods, numerous studies have applied neural networks for gas analysis. The neural networks used in the previous studies mainly include the back-propagation artificial neural network (BP-ANN), the radial basis function neural network (RBFNN), and the convolutional neural network (CNN) [23–27]. BP-ANN uses the back propagations algorithm with a simple structure. It needs the manual feature extraction to reduce the dimension of spectral data; otherwise it would be difficult to converge because it has too many parameters. RBFNN converges quickly, but using the manual feature extraction is also inevitable [28, 29]. In the aforementioned neural networks, the manual extraction of features increases the complexity of the experiment [30, 31]. In contrast, CNN adds convolutional layers to extract features automatically and greatly reduces the workload; therefore, CNN is more suitable for gas detection [32–35].

We propose a hierarchical CNN model with two modules to detect the strong and weak absorption gas separately. The strong absorption gas has priority for detection, and its prediction results are used to adjust the input of the module which detects the weak one. In our experiment, mixtures of SO_2, NO_2, and NH_3 are analyzed. SO_2 and NO_2 are the detected gases, while NH_3 is the interfering gas. For the simulation samples, the average absolute errors are 0.5 and 0.9 ppm for SO_2 and NO_2, respectively. For the experimental samples, the model performs well when the absorption intensities of components differ by no more than one order of magnitude. The proposed model is more suitable for high-concentration gas mixtures and the prediction accuracy increases when the signal-to-noise ratio is higher than 80. Compared with the single-module CNN model, the hierarchical structure can make a remarkable improvement in the prediction accuracy of a weak absorption gas. The simulation results also show that the proposed model can be extended to the case when other interfering gases are present. In conclusion, our model has proved to be feasible for the quantitative analysis of gas mixtures.

Theories and methods. The Beer–Lambert law is

$$A(\lambda_i) = \sum_{j=1}^{j=n} Lc_j \sigma(\lambda_{ij}) \binom{i=1,2,3,\ldots m}{j=1,2,3,\ldots n} = \ln(1/T), \quad (1)$$

where c_j (mol/cm^3) and $\sigma(\lambda_{ij})$ (cm^2/mol) are the concentration of the jth gas and its absorption cross-section at a wavelength λ_i. The sum of the absorbance of each component constitutes $A(\lambda_i)$, which represents the absorbance of the mixed gas. An amount of N_2 is selected as the diluent gas, T is the ratio of the transmittance between the gas mixture and N_2. L is the optical path and is set to 10 cm in our experiment.

In our experiment, mixtures of SO_2, NO_2, and NH_3 are analyzed. SO_2 and NO_2 are the detected gases, while NH_3 is the interfering gas. Since the three gases have distinct absorption characteristics at 200–350 nm, we chose this band for concentration inversion. The spectrophotometer (UV-3600, Shimadzu) with a resolution of 0.01 nm is used to measure the transmission spectrum. The transmittance of N_2 is shown in Fig. 1. It can be seen that the transmittance spectrum is easily affected by the instrument noise.

Gases with specific concentrations can be configured according to the following equation:

$$C = C_0 \frac{Q_0}{Q_0 + Q}, \quad (2)$$

where C_0 and C are the initial and configured concentrations of the gas; Q_0 and Q are the flow rates of the detected gas and the diluent gas, respectively (N_2 is chosen for our study). The diagram of the gas distribution device is shown in Fig. 2. Firstly, the average transmission spectrum is obtained by multiple measurements, while, secondly, its absorption cross-section is calculated according to the Beer–Lambert law.

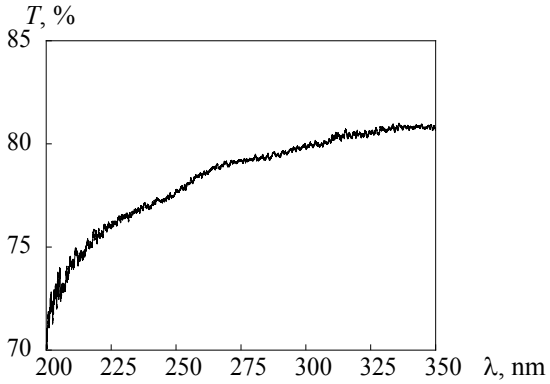

Fig. 1. Transmittance spectrum of N_2.

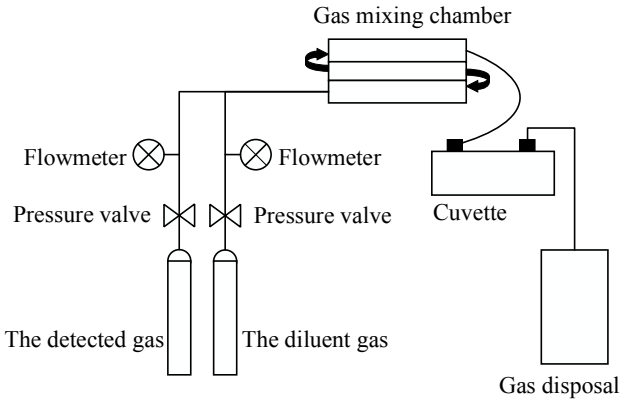

Fig. 2. Diagram of the gas distribution device.

After the steps in Fig. 2, the absorption cross-sections of SO_2, NO_2, and NH_3 are obtained, as shown in Fig. 3. It can be seen that the absorption cross-section of SO_2 has intensive spectral features in the ranges of 200–230 and 260–320 nm, while NH_3 has discrete absorption peaks with high intensity in the range of 200–225 nm. In comparison, the absorption intensity of NO_2 is much smaller and there are no obvious peaks and valleys in the detection band, indicating that its absorption is weak.

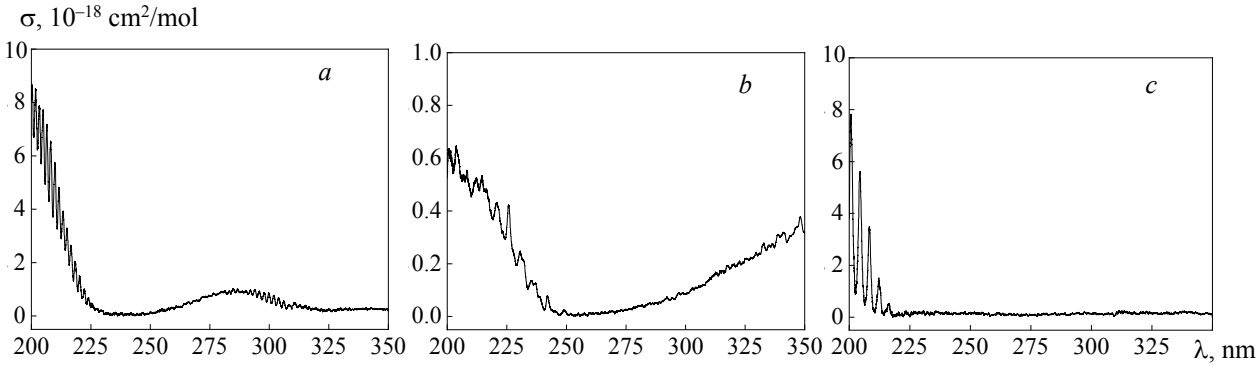

Fig. 3. Measured absorption cross sections of (a) SO_2, (b) NO_2, and (c) NH_3.

The gas absorption spectrum contains the absorption characteristics from which the CNN model can perform automatic feature extraction. Figure 4 shows that the CNN model consists of three parts – the input layer, the hidden layer, and the output layer. The input layer receives one-dimensional (1D) absorbance spectra. The hidden layer is used for feature extraction and consists of a convolutional layer, a max-pooling layer, and a fully-connected layer. In the convolutional layer, the convolution kernel is a weight matrix sequential-

ly multiplied with the input data to extract features. The extracted features are compressed in the max-pooling layer to reduce the dimension. The mapping relationship between the compressed features and the true concentration is learned in the fully connected layer. Finally, the predicted concentration is output from the output layer.

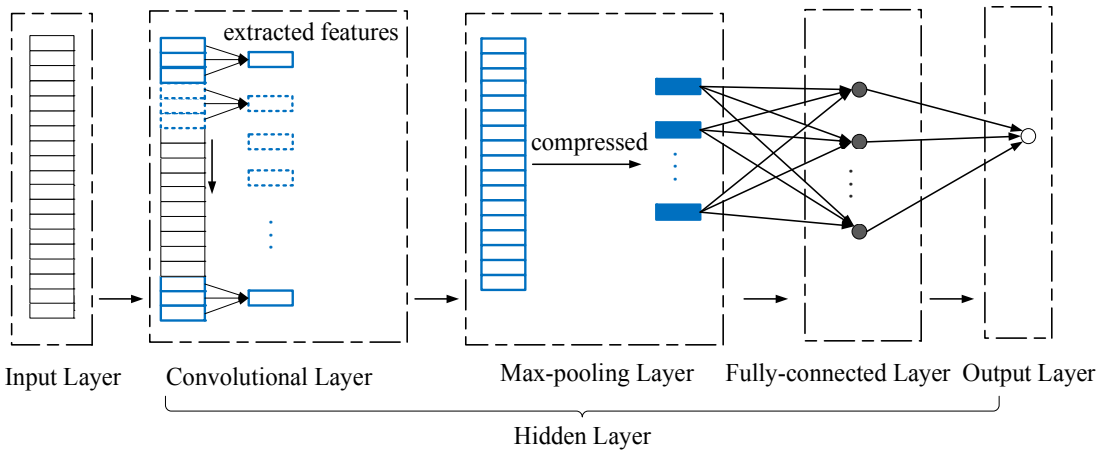

Fig. 4. Framework of CNN.

As can be seen from Fig. 3, SO_2 has denser spectral characteristics, indicating that its absorption would seriously interfere with the NO_2 during gas detection. Herein, the hierarchical CNN model is proposed to resolve this problem and work on improving the prediction accuracy of a weak absorption gas. The flowchart is illustrated in Fig. 5. The greatest superiority of the proposed model over other models is that it is divided into two modules: the output of module 1 is used to adjust the spectrum provided to module 2. The hierarchical CNN model contains the following three main steps:

1. The one-dimensional absorbance spectrum of the gas mixture is input to module 1, in which only the concentration of the strong absorption gas is predicted.

2. The theoretical absorbance spectrum of the strong absorption gas is calculated based on its prediction, then subtracted from the original spectrum to obtain the residual spectrum.

3. Input of the residual spectrum into module 2. The second CNN module is used to predict the concentration of the weak absorption gas.

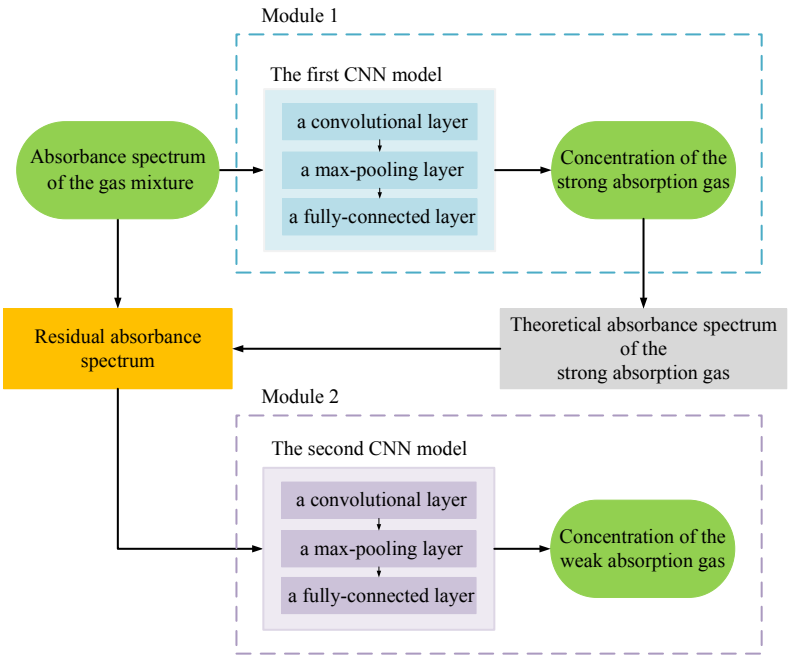

Fig. 5. Flowchart of the hierarchical CNN model.

The loss function is used to estimate the disparity between the predicted and true values. In the multi-output neural network, it is the sum of the loss functions of all outputs. The loss function of the hierarchical CNN model is

$$\text{Loss} = w_1\text{Loss1} + w_2\text{Loss2}, \quad (3)$$

where Loss is the total loss function, and Loss1 and Loss2 are the loss functions of modules 1 and 2. Since the output of module 1 is used to adjust the spectrum provided to module 2, we set its loss function to a higher weight: w_1 ($w_1 > w_2$). In this case, the prediction of the strong absorption gas can be better optimized during the training process, which causes a more accurate residual spectrum, thus improving the prediction accuracy of the weak absorption gas. After the comparison, it is found that the prediction results are optimum when w_1 was set to 1 and w_2 was set to 0.5.

Implementation details. *Composition of simulation dataset.* In our experiment, mixtures of SO_2, NO_2, and NH_3 are analyzed, with NH_3 being the interfering gas. Because SO_2 has a higher absorption intensity, it is regarded as the strong absorption gas, while NO_2 is the weak one. Their concentrations are predicted in modules 1 and 2, respectively. Neural networks require a large number of training and test samples. The training samples are only involved in the training process, while the test samples are used to verify the performance of the trained model. The measured absorption cross-sections are used to generate simulated sample spectra according to Eq. (1), where the concentrations are set randomly. The composition of the simulation dataset is given in Table 1.

TABLE 1. Composition (Range of Concentration, ppm) of the Simulation Dataset

Composition	Number of sample	Detected gas		Interfering gas
		SO_2	NO_2	NH_3
Training samples	20000	0–2000	0–2000	0–2000
Test samples	10000	0–2000	0–2000	0–2000

Hyper-parameters section. The log-cosh loss function combines the advantages of the mean squared error (MSE) and the mean absolute error (MAE). It has a fast error convergence and is independent of abnormal points. Therefore, it is chosen for our study, and the definition is shown in the following equation:

$$L(y, y_i) = \sum_{i=1}^{n} \log(\cosh(y - y_i)) . \quad (4)$$

Let us suppose that n samples are sent into the hierarchical CNN model for training. For the ith sample, y and y_i are its true and predicted values, respectively, and $y - y_i$ represents the error between them.

All the training samples in Table 1 are applied to train the proposed model, and Table 2 shows its performance with different hyperparameter combinations. A smaller loss value indicates a better prediction. Based on this, the size of the convolution kernel is set to 4 and its sliding stride is set to 8 in our model.

TABLE 2. Performance of the Model with Different Hyperparameter Combinations

Model	Parameters of the convolution kernel		Log-Cosh loss value	
	Sliding stride	Size	Module 1	Module 2
1	2	2	0.16	0.53
2	2	4	0.98	0.95
3	2	6	1.20	1.62
4	2	8	0.16	0.52
5	4	4	0.17	0.83
6	6	4	1.26	1.01
7	8	4	0.16	0.48
8	16	4	0.88	1.22

Details of the hierarchical CNN model. The 1D spectral data of size (15000,1) are input to the model. The number of convolution kernels is 2, the boundary filling method is *valid*, and the regularization method is l_2. The size of the pooling kernel is 9 and its step size is 8. The number of neurons in the fully connected layer is 36. The specific details of the hierarchical model are shown in Fig. 6.

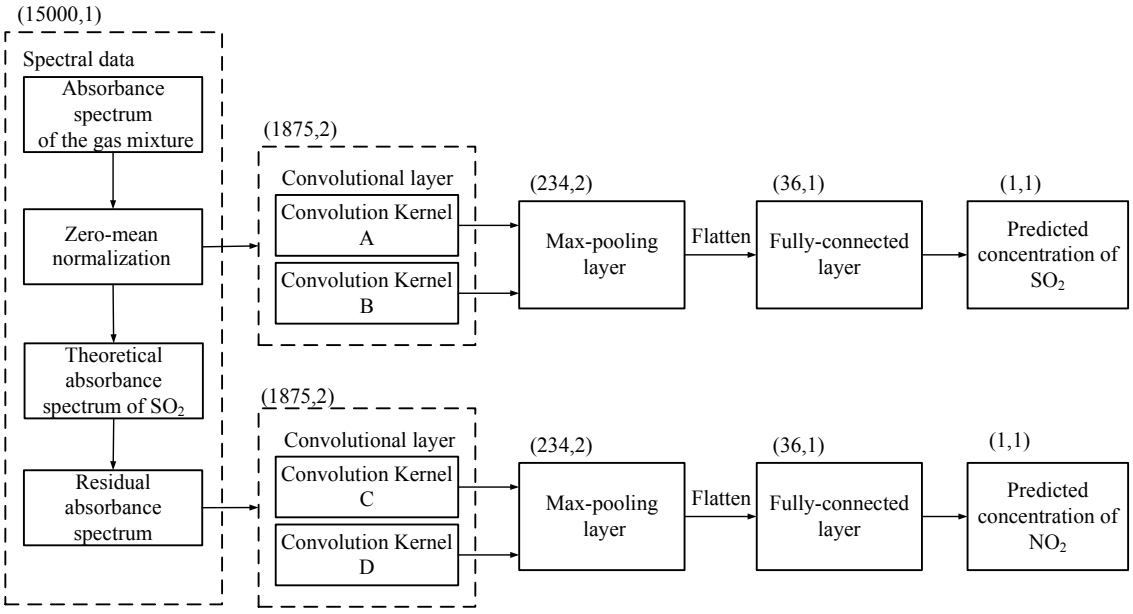

Fig. 6. Details of the hierarchical CNN model.

Results and discussion. The architecture of the single-module CNN model is shown in Fig. 7. As compared with hierarchical CNN model, it has only one output to predict concentrations of SO_2 and NO_2 simultaneously.

The single-module and the hierarchical CNN models are trained separately with simulation training samples, and the training process is shown in Fig. 8. One can see that the training effect of the hierarchical structure is much better.

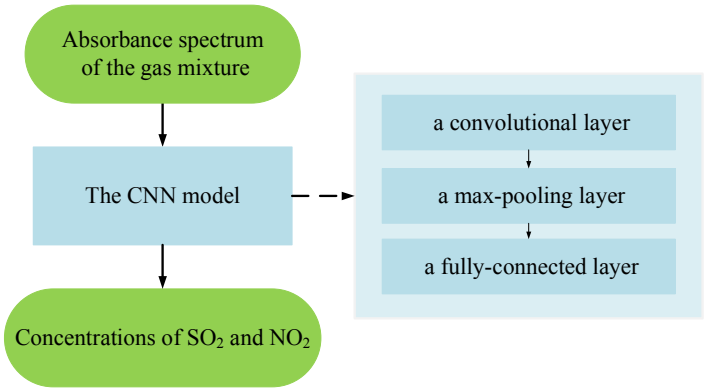

Fig. 7. Architecture of the single-module CNN model.

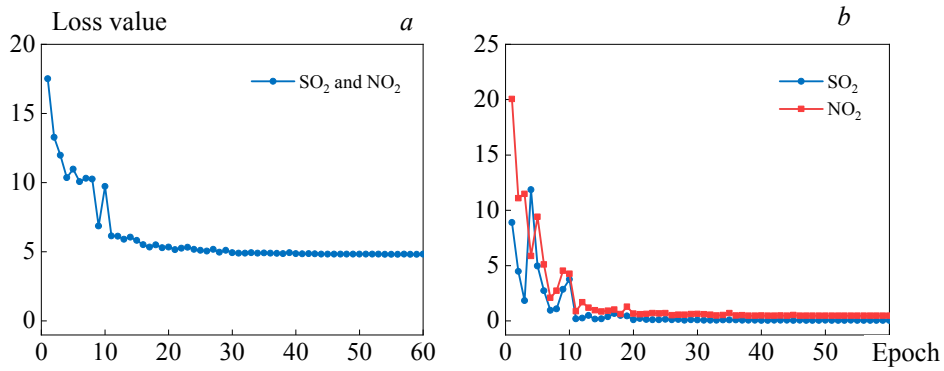

Fig. 8. Training process of (a) the single-module CNN model, and (b) the hierarchical CNN model.

The test samples are applied to the two trained models and Fig. 9 shows the prediction error distribution. One can find that the hierarchical CNN model has more samples within a small error range. The average absolute errors of the single-module model for SO_2 and NO_2 are 1.5 and 1.6 ppm, respectively, while they are 0.5 and 0.9 ppm for the hierarchical CNN model.

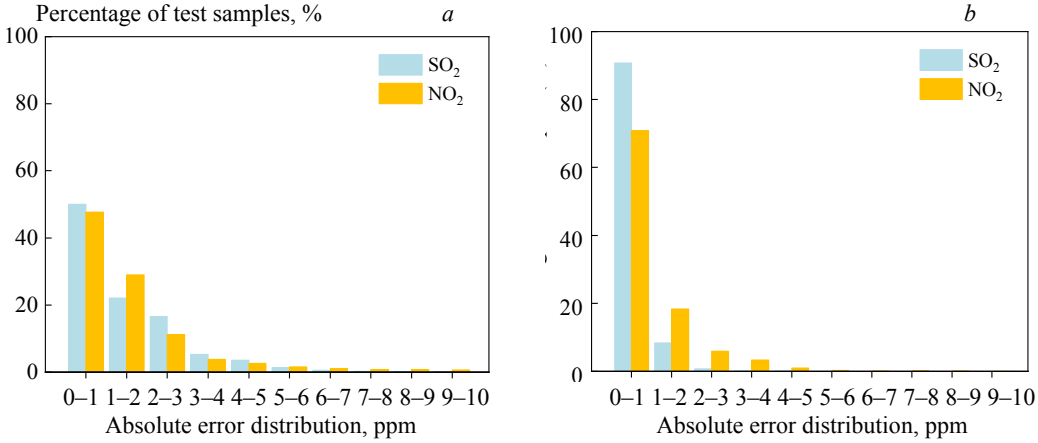

Fig. 9. The sample error distribution for (a) the single-module CNN model, and (b) the hierarchical CNN model.

We also configured samples with different concentrations to verify their predictive effect for experimental samples. The prediction results are recorded in Tables 3 and 4. The results show that the hierarchical CNN outperforms the single-module CNN in predicting the concentration of NO_2, indicating that the hierarchical structure can achieve promising performance in reducing cross-interference and ameliorating the prediction accuracy of weak absorption gas.

TABLE 3. Prediction Results of the Single-Module CNN Model for Experimental Samples

Sample	True value, ppm			Predicted value, ppm		Relative error, %	
	SO_2	NO_2	NH_3	SO_2	NO_2	SO_2	NO_2
1	90	110	0	97.7	121.8	8.6	10.7
2	215	190	0	223.0	199.1	3.7	4.8
3	450	513	0	460.1	525.7	2.2	2.5
4	98	101	110	106.4	115.1	8.6	14.0
5	195	206	190	187.2	225.5	4.0	9.5
6	469	490	478	460.1	502.2	1.9	2.5
7	190	1958	179	186.0	1961.5	2.1	0.2
8	200	205	1933	212.3	255.5	6.2	24.6
9	2000	212	180	1979.8	253.3	1.0	19.5

TABLE 4. Prediction Results of the Hierarchical CNN Model for Experimental Samples

Sample	True value, ppm			Predicted value, ppm		Relative error, %	
	SO_2	NO_2	NH_3	SO_2	NO_2	SO_2	NO_2
1	90	110	0	94.2	118.1	4.7	7.4
2	215	190	0	220.1	194.2	2.4	2.2
3	450	513	0	454.7	516.8	1.0	0.7
4	98	101	110	104.6	108.0	6.7	6.9
5	195	206	190	187.0	195.4	4.1	5.1
6	469	490	478	462.9	480.4	1.3	2.0
7	190	1958	179	186.5	1950.7	1.8	0.4
8	200	205	1933	206.1	221.6	3.1	8.1
9	2000	212	180	1968.7	245.2	1.6	15.7

The predictions of samples 1–6 in Table 4 show that the prediction error of the model increases when the interfering gas is added. The errors are still acceptable, which proves that our model has good resistance to interference. Since the absorption cross-section of NO_2 is one order of magnitude smaller than that of the other two gases, the absorption intensities of components differ by two orders of magnitude in samples 8 and 9, which reduces the prediction accuracy of NO_2. As for sample 7, the absorption intensities are comparable and the model predicts well. The experimental results in Table 4 show that the proposed model is more suitable when the absorption intensities of the components differ by no more than one order of magnitude.

To analyze the detection limit of the proposed model, we apply it to the low concentration sample (sample 10: SO_2 48 ppm, NO_2 66 ppm, NH_3 55 ppm) – for this sample, the predicted SO_2 and NO_2 are 60.6 and 80.7 ppm, and their absolute errors are 12.6 and 14.7 ppm, respectively. When the concentrations of the components increase to 100 ppm, taking sample 4 as an example (SO_2 98 ppm, NO_2 101 ppm, NH_3 110 ppm), the prediction of SO_2 and NO_2 are 104.6 and 108.0 ppm with absolute errors 6.6 and 7.0 ppm, respectively. The absorbance spectrum and extracted measurement noise of the two samples are shown in Fig. 10. The measurement noise is obtained by the moving window average method. As can be seen from the figures, the ratio of the maximum signal to maximum noise (SNR) is about 59 for sample 10 and about 80 for sample 4. The prediction results show that the model predicts better when the SNR is higher than 80. Therefore, the use of high-resolution instruments can improve the SNR and increase the accuracy of predictions.

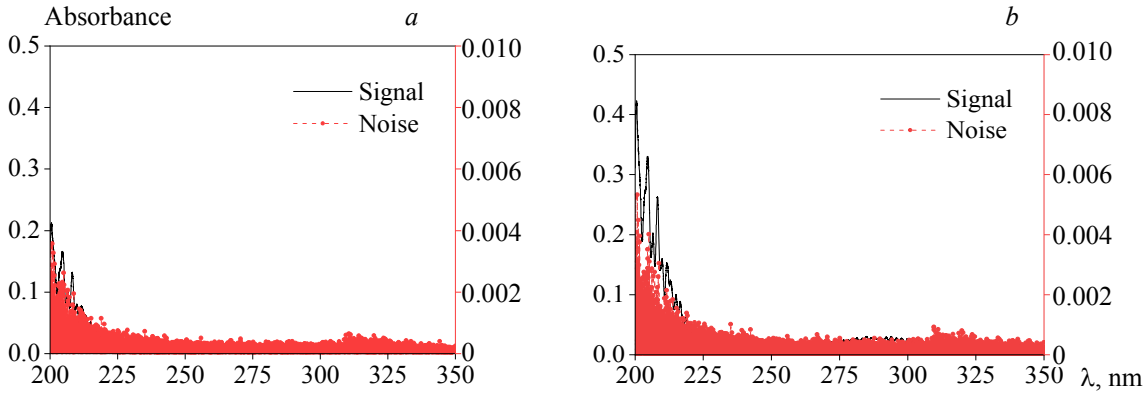

Fig. 10. Signal and noise in the absorbance spectrum of (a) sample 10, (b) sample 4.

Furthermore, a simulation experiment is conducted to test the applicability and stability of the proposed model. In addition to NH_3, O_3, and H_2S are added as interfering gases to increase the intensity of interference. In this experiment, the simulation samples are generated based on the standard absorption cross-sections. The composition of the simulation dataset is shown in Table 5 [36–40].

TABLE 5. Composition (Range of concentration, ppm) of Simulation Dataset in the Presence of other Interfering Gases

Composition	Number of sample	Detected gas		Interfering gas		
		SO_2	NO_2	NH_3	O_3	H_2S
Training samples	20000	0–2000	0–2000	0–2000	0–2000	0–2000
Test samples	10000	0–2000	0–2000	0–2000	0–2000	0–2000

Figure 11 shows the training process of the hierarchical CNN model in the presence of the three interfering gases. For the test samples, the average prediction errors are 0.8 and 1.4 ppm for SO_2 and NO_2, respectively. The simulation results demonstrate that the proposed model is still reliable for the situation when other interfering gases exist.

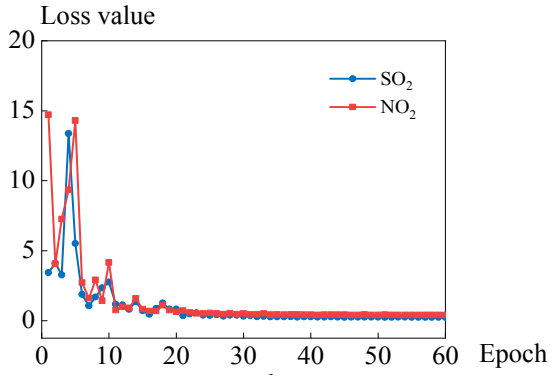

Fig. 11. Training process of the hierarchical CNN model in the presence of other interfering gases.

Conclusions. We presented a hierarchical CNN model for mixed gas concentration inversion by analyzing the absorption spectrum in the ultraviolet spectral range. The results show that the detection accuracy of a weak absorption gas can be improved by setting different weights on the loss functions of the hierarchical structure. More sophisticated measuring instruments can be used to reduce instrument noise and make the simulated spectral data closer to the true values. We believe that our model can be an effective approach that provides a broad application prospect for the analysis of gas mixtures.

Acknowledgements. This research was funded by the National Natural Science Foundation of China (NSFC) (No. 11874107). The authors have no relevant financial or nonfinancial interests to disclose.

REFERENCES

1. H. Amal, D. Shi, R. Ionescu, W. Zhang, Q. Hua, Y. Pan, L. Tao, H. Liu, H. Haick, *Int. J. Cancer*., **136**, No. 6, E614–E622 (2015).
2. T. Xu, C. Tang, T. Yang, W. Zhu, J. Liu, *Int. J. Rock Mech. Min. Sci*., **43**, No. 6, 905–919 (2006).
3. Y. Zhang, H. Guo, Z. Lu, L. Zhan, P. Hung, *Eng. Appl. Art. Intell*., **92**, 103643 (2020).
4. M. Schroter, A. Obermeier, D. Bruggemann, M. Plechschmidt, O. Klemm, *J. Air Waste Manage. Ass*., **53**, No. 6, 716–723 (2003).
5. J. H. Yang, J. Jung, J. H. Ryu, J. J. Yoh, *Chemosphere*, **257**, 127237 (2020).
6. M. Lassen, D. B. Harder, A. Brusch, O. S. Nielsen, D. Heikens, S. Persijn, J. C. Petersen, *Opt. Express*, **25**, No. 3, 1806–1814 (2017).
7. J. Uotila, V. Koskinen, J. Kauppinen, *Vib. Spectrosc*., **38**, No. 1-2, 3–9 (2005).
8. H. O. Edwards, J. P. Dakin, *Sens. Act. B: Chem*., **11**, No. 1-3, 9–19 (1993).
9. J. Kong, N. R. Franklin, C. Zhou, M. G. Chapline, S. Peng, K. J. Cho, H. Dai, *Science*, **287**, No. 5453, 622625 (2000).
10. S. Herberger, M. Herold, H. Ulmer, A. Burdack-Freitag, F. Mayer, *Build. Environ*., **45**, No. 11, 2430–2439 (2010).
11. V. Kampitakis, E. Gagaoudakis, D. Zappa, E. Comini, E. Aperathitis, A. Kostopoulos, G. Kiriakidis, V. Binas, *Mat. Sci. Sem. Proc.*, **115**, 105149 (2020).
12. P. Mahbub, A. Noori, J. S. Parry, J. Davis, A. Lucieer, M. Macka, *Talanta*, **218**, 121144 (2020).
13. Z. Bielecki, T. Stacewicz, J. Smulko, J. Wojtas, *Appl. Sci.-Basel*., **10**, No. 15, 5111 (2020).
14. L. Shao, B. Fang, F. Zheng, X. Qiu, Q. He, J. Wei, C. Li, W. Zhao, *Spectrochim. Acta A*, **222**, 117118 (2019).
15. L. Dong, F. K. Tittel, C. Li, N. P. Sanchez, H. Wu, C. Zheng, Y. Yu, A. Sampaolo, R. J. Griffin, *Opt. Express*, **24**, No. 6, A528–A535 (2016).
16. J. Zhao, S. Xiao, *Optik*, **195**, 163142 (2019).
17. S. Khan, D. Newport, S. Le Calvé, *Sensors*, **19**, No. 23, 5210 (2019).
18. L. Mei, P. Guan, Z. Kong, *Opt. Express*, **25**, No. 20, A953–A962 (2017).
19. G. Hönninger, C. von Friedeburg, U. Platt, *Atm. Chem. Phys*., **4**, No. 36, 231–254 (2004).
20. J. Mellqvist, A. Rosen, *J. Quant. Spectrosc. Radiat. Transfer*, **56**, No. 2, 209–224 (1996).
21. S. Determann, J. M. Lobbes, R. Reuter, J. Rullkotter, *Mar. Chem*., **62**, No. 1-2, 137–156 (1998).
22. Y. Matsumi, H. Shigemori, K. Takahashi, *Atm. Environ*., **39**, No. 17, 3177–3185 (2005).

23. J. Yang, L. Du, Y. Cheng, S. Shi, C. Xiang, J. Sun, B. Chen, *Opt. Express*, **28**, No. 13, 18728–18741 (2020).
24. C. L. Hammer, G. W. Small, R. J. Combs, R. B. Knapp, R. T. Kroutil, *Anal. Chem*., **72**, No. 7, 1680–1689 (2000).
25. M. Caselli, L. Trizio, G. de Gennaro, P. Ielpo, *Water Air Soil Poll*., **201**, No. 1-4, 365–377 (2009).
26. A. A. Tomchenko, G. Harmer, B. Marquis, J. Allen, *Sens. Act. B: Chem*., **93**, No. 1-3, 126–134 (2003).
27. L. Song, H. Wu, Y. Yang, Q. Guo, J. Li, *Appl. Opt.*, **59**, No. 17, E9–E16 (2020).
28. J. Wang, M. Shi, P. Zheng, Sh. Xue, R. Peng, *J. Appl. Spectrosc*., **85**, 190–196 (2018).
29. S. Cui, J. Wang, L. Yang, J. Wu, X. Wang, *J. Pharm. Biomed. Anal*., **102**, 64–77 (2015).
30. Y. Yu, Y. Qu, *Optik*, **217**, 164915 (2020).
31. L. Xiao, K. Tong, L. Song, L. Wang, P. Wu, W. Liu, X. Zhao, *Opt. Eng*., **59**, No. 12, 125101 (2020).
32. X. Wang, Z. Li, D. Zheng, W. Wang, *J. Appl. Spectrosc*., **87**, 54–61 (2020).
33. Y. Chen, H. Jiang, C. Li, X. Jia, P. Ghamisi, *J. Geosci. Remote*, **54**, No. 10, 6232–6251 (2016).
34. L. Jing, M. Zhao, P. Li, X. Xu, *Measurement*, **111**, 1–10 (2017).
35. W. Wang, Y. Yang, X. Wang, W. Wang, J. Li, *Opt. Eng*., **58**, No. 4, 040901 (2019).
36. S. L. Manatt, A. L. Lane, *J. Quant. Spectrosc. Radiat. Transfer*, **50**, 267–276 (1993).
37. W. Schneider, G. K. Moortgat, J. P. Burrows, G. S. Tyndall, *J. Photochem. Photobiol. A: Chem*., **40**, 195–217 (1987).
38. B. M. Cheng, H. C. Lu, H. K. Chen, M. Bahou, Y. P. Lee, A. M. Mebel, L. C. Lee, M. C. Liang, Y. L. Yung, *Astrophys. J*., **647**, 1535–1542 (2006).
39. J. Brion, A. Chakir, D. Daumont, J. Malicet, C. Parisse, *Chem. Phys. Lett*., **213**, 610–612 (1993).
40. H. Grosch, A. Fateev, S. Clausen, *J. Quant. Spectrosc. Radiat. Transfer*, **154**, 28–34 (2015).